Journal of Applied Biology & Biotechnology Vol. 6(2), pp. 6-14, Mar-Apr, 2018
Available online at http://www.jabonline.in
DOI: 10.7324/JABB.2018.60202

ZnS nanoparticles persuade alterations in metabolic and hematological aspects in the cyprinid *Labeo bata* (Hamilton, 1822)

Nilanjana Chatterjee[1], Baibaswata Bhattacharjee[2]*

[1]Department of Zoology, Ramananda College, Bishnupur, Bankura, India, [2]Department of Physics, Ramananda College, Bishnupur, Bankura, India.

ARTICLE INFO

Article history:
Received on: July 18, 2017
Accepted on: December 08, 2017
Available online: February 17, 2018

Key words:
ZnS nanoparticles,
Hypoxia,
Acclimatization,
Labeo bata

ABSTRACT

Due to increased surface photo-oxidation property associated with the nanocrystalline form of ZnS, the dissolved oxygen content in water gets reduced in a dose-dependent manner from their normal values when different concentrations of ZnS nanoparticles (NPs) with various sizes are exposed to the water. Therefore, the animals living in a habitat exposed to ZnS NPs are forced to live in a hypoxic atmosphere. The mechanism of acclimatization to this hypoxic atmosphere by an Indian minor carp *Labeo bata*, along with its liver morphology, hematological parameters, and metabolic responses are studied systematically. During progressive hypoxia, the liver histomorphology of *L. bata* shows salient alterations from its normal tissue layout. Furthermore, a significant increase in the number density of red blood corpuscles (RBC) is documented for relatively smaller time (<12 days) of ZnS NP exposure. Under hypoxia condition, hemoglobin and hematocrit concentrations are found to show a characteristic feature showing a peak value for an exposure time of 9 days. Blood glucose and blood lactate levels of *L. bata* are found to vary in accordance with the varied physiological behavior of the fish under ZnS NP exposure.

1. INTRODUCTION

Applications of a wide range of products containing nanoscale materials (1–100 nm) are obvious in our day-to-day life of late [1-3]. The augmenting production of nanoparticles (NPs) and its snowballing uses are quite responsible for the exposure of such materials in watercourses either industrial or medical waste or as domestic and urban water sewage allowing nanoscale products and byproducts to enter the aquatic environment. Due to their small size and very high surface to volume ratio, NPs possess modified physical and chemical properties compared to their bulk counterparts. NPs are theoretically expected to be more toxic for their greater surface reactivity, and their ability of penetration and accumulation within cells and organisms [4-6] is a matter of great concern. Direct ingestion and entry through gills, olfactory organs or body wall can be identified as some of the potentials routes of up taking NPs by aquatic organisms [7-9]. All these have unknown consequences for aquatic life.

Recent studies [10-14] have shown several perilous effects of diverse NPs on fish. Carbon nanotubes (CNT) are identified as a respiratory toxicant in rainbow trout [15]. Fullerenes (C_{60}) are shown to be detrimental for aquatic environments [16-21]. Fullerenes are reported to cause oxidative damage in largemouth bass (*Micropterus salmoides*) [16]. It is found that the copper NPs affect the gills of Zebrafish (*Danio rerio*) through a mechanism that is different from that the dissolved copper ions [22]. Exposure of TiO_2 NPs to rainbow trout (*Oncorhynchus mykiss*) [23] results in various sublethal effects including respiratory problems in the fish.

The ZnS NPs, when exposed to water, have shown to make some changes in the physicochemical parameters of the water such as dissolved oxygen level and pH, due to their enhanced photo-oxidation property associated with their NP character [24-31]. As ZnS NPs reduce the level of dissolved oxygen content in water, fish are forced to face hypoxia in their habitat [25-31] resulting abnormal growth and maturity in *Mystus vittatus* [25,26,29,31] and showing adverse effect on different organs of *Labio bata* [27], *M. vittatus* [26], and *Mystus tengara* [28,30].

In many cases, the industries are being cropped up without preparing a proper system for disposal of sewage. The wastes from different industries contain mostly sulfide NPs. ZnS is one of such materials that can be found in the wastes of rubber, cosmetic, and pharmaceutical industries. Therefore, it is now gradually becoming very important to detect the hazardous effect of ZnS NPs on aquatic animals.

L. bata is prevalently an edible fish in eastern India and Bangladesh. Therefore, any perilous effect on this fish will reduce its production creating a negative impact on the commercial fish market. Keeping this in mind, the present study is designed for systematic identification of the adverse effect of ZnS NP on the metabolic and hematological parameters of *L. bata* to avoid the situation of economic loss.

*Corresponding Author
Baibaswata Bhattacharjee, Department of Physics,
Ramananda College, Bishnupur - 722 122, Bankura, India.
Email: baib23@gmail.com

2. MATERIALS AND METHODS

2.1. Synthesis and Characterization of ZnS NPs

A simple wet chemical method is used to synthesize ZnS NPs. A solution of $Zn(NO_3)_2.6H_2O$ (purified, Merck, India) in 2-propanol $(CH_3)_2CHOH$ (GR, Merck India) dried over activated molecular sieve zeolite 4A, and distilled water is used as the zinc precursor. The alcohol and water volume ratio is maintained as 1:5 throughout while preparing the solution. This solution is stirred for 2 h. Sodium sulfide (Na_2S, purified, Merck, India) dissolved in distilled water after 2 h of stirring is used as the sulfur precursor. To attain the required stoichiometry in the synthesized ZnS NPs, the molar ratio of Zn and S is maintained as 1:1 in the precursors.

During the synthesis, Na_2S solution is quickly injected into the $Zn(NO_3)_2.6H_2O$ solution. Immediate formation of ZnS NP colloid is observed in this method. Controlling the reaction temperature different sized of ZnS NPs are synthesized. After completion of the reaction, the precipitates are centrifuged and washed several times with deionized water, ethanol, and acetone. A vacuum oven is used to dry the samples at 30°C, and then those are kept in vacuum for further use.

A Hitachi H-7100 microscope operated at 100 kV is employed to perform the transmission electron microscopy (TEM). Powder dispersed in ethanol is placed carefully on the carbon coated Cu grid and subsequently dried for TEM study. The size distribution histogram is obtained using a particle size analyzer (PSA) (Nano-S, Malvern, Worcestershire, UK). A MAC M03 diffractometer is employed for the X-ray diffraction study (XRD) using Ni-filtered Cu Kα radiation (λ = 0.154056 nm) at 40 kV, 30 mA. A scanning speed of 2°/min is fixed while carrying out the $\theta/2\theta$ scan in the 2θ range of 20–60°. Hitachi S-2400 instrument is used to perform energy dispersive X-ray (EDX) study. A commercial VG Microtech (MT-500) machine using Al Kα radiation is employed for X-ray photoelectron spectroscopic (XPS) study. The C1s peak appeared at 284.6 eV is used as the internal standard for all the samples. The peak position in each case is normalized with respect to the C1s peak. Calibration in charge correction is done from the observed C1s binding energy.

2.2. Measurement of Dissolved Oxygen Content and pH Value of Water

Properly calibrated electronic lab meters with probes having accuracy level up to one decimal point are used to measure the dissolved oxygen content and pH value of water under control and different experimental conditions.

2.3. Fish Husbandry

Matured male and female *L. bata* specimens are collected from local fishermen and immediately transferred to watertight containers containing tap water that has been disinfected and allowed to stand for a few days. The arrangement is provided with necessary oxygen supply. The temperature of the water is maintained within the range of 25–30°C to create the natural environment. Small quantity of natural fish food is supplied to the fish in regular interval. The fishes are acclimatized with the laboratory environment for 60 days before the toxicity experiments are started.

2.4. Toxicity Test

Five concentrations (σ = 100, 250, 500, 750, and 1,000 µg/L) of the ZnS NPs of diverse sizes (d = 3, 7, 12, and 20 nm) are applied to the habitat of the fish specimens for 36 days. The concentration of NP that resulted in a maximum departure from the controlled condition is identified through trial experiments. After this range is attained, the effect of time of exposure of ZnS NPs on *L. bata* is studied extensively.

2.5. Histological and Histometric Studies

After the controlled and treated fish are sacrificed; the liver tissue is dissected out and subjected to routine histological procedures. Upgrading or dehydration of tissues is done by putting them for 10 min each (2 changes) in distilled water, 30%, 50%, 70%, and 90% ethanol, and finally absolute alcohol (100% ethanol). Dehydration using upgraded alcohol is followed by xylene treatment, paraffin embedding (melting point 56–58°C), section cutting (4 µm), and staining using Delafield's Hematoxylin and Eosin (HE) before they are observed under a compound light microscope at different desired magnifications (×400, ×600, ×800) and photographed with a digital camera. The morphometry of hepatic tissue is done using reticulo micrometer and ocular micrometer attached to the compound light microscope. Each measurement is made 5 times and their mean value is used for any analysis.

2.6. Determination of the Metabolic Parameters

Blood samples are collected from fishes living under control and different experimental conditions by puncturing the dorsal aorta using 20 G×1.5 disposable syringes and collected in microtubes. After collection, the samples are used immediately to determine the metabolic parameters. Five-fold measurement is done for each sample, and the mean is taken as the result for greater accuracy. Blood glucose levels are measured using a properly calibrated portable blood glucose analyzer (ACCU-Chek Active, Roche Diagnostics GmbH, Mannheim, Germany), and blood lactate levels are measured using a properly calibrated portable blood lactate analyzer (Accusport, Boehringer Mannheim, Germany).

2.7. Hematological Study

Blood samples are obtained from 20 different fish samples by puncturing the caudal vein using a 20 G×1.5 disposable syringe and collected in microtubes having ethylenediaminetetraacetic acid (ratio 1.26 mg/0.6 ml) as the anticoagulant agent. For the blood film preparation, a drop of blood is put on the edge of a clean grease free slide, and the blood film is spread over it uniformly in a horizontal direction by means of a spreader. The blood film is air dried and then stained with Leishman's stain for counting and depicting the RBCs. All the hematological profiles are calculated within 1 h of blood sample collection with the help of a HeCo Vet C blood cell counter (Italy). Parameters such as the hemoglobin concentration (Hgb), hematocrit (Hct) value, and red blood cell count (RBC) are determined by evaluating the hemogram.

2.8. Statistical Analysis and Curve Fitting

All data are expressed as means ± SE. One-way analysis of variance is run to compare the differences between groups treated under different experimental conditions and control groups. Differences are considered statistically significant when $P < 0.05$. Curve fitting to the experimentally obtained data is done using the software Origin 9.

3. RESULT AND DISCUSSION

3.1. Microstructural and Compositional Study of ZnS NPs

TEM of a representative ZnS NP sample with the corresponding selected area diffraction pattern is shown in Figure 1a. Conspicuous presence

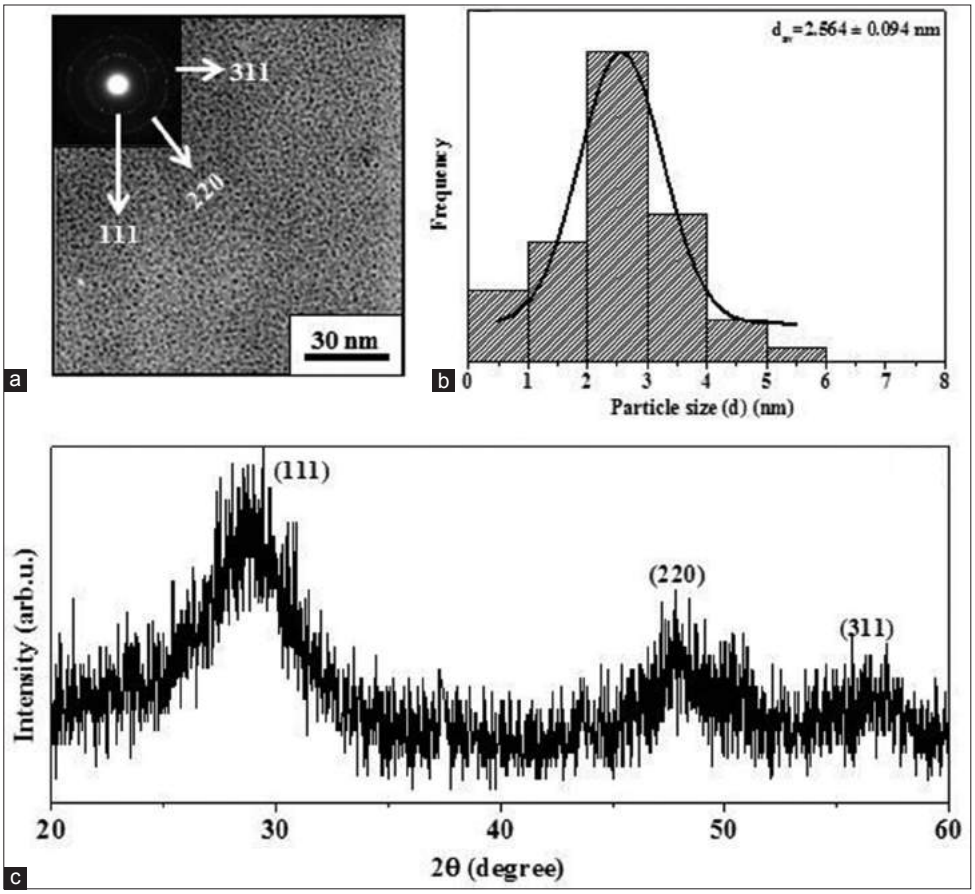

Figure 1: (a) Transmission electron micrograph of representative ZnS nanoparticles and (inset) the corresponding diffraction pattern, (b) particle size analysis data of the same representative sample, (c) X-ray diffraction pattern of the same representative sample.

of very small ZnS NPs is easily identified from the micrograph. The diffraction pattern shows a central halo with concentric ring patterns. The rings can be attributed to the reflections from (111), (220), and (311) planes. This observation confirms the cubic crystallographic structure of the ZnS NPs. The average size (d_{av}) of the nanocrystallites determined from TEM is around 3 nm (±0.5 nm). Narrow size distribution of the particles is seen from the PSA data [Figure 1b]. The corresponding fitting curve reveals d_{av}~2.6 nm (±0.1 nm). This result tallies well with the TEM result.

Figure 1c demonstrates the XRD spectrum of the same representative ZnS NP sample. Prominent peaks from (111), (220), and (311) planes confirms the formation of cubic crystalline phase. This observation is in agreement with the electron diffraction results. Broadening of the XRD peaks can be attributed to the small size of the ZnS NPs present in the sample. The crystallite size is obtained as 3.04 nm from the XRD data using the Debye equation. This value tallies well with the TEM and PSA results.

EDX measurements are used to determine the chemical compositions of the ZnS NPs. Using the EDX data, the Zn/S ratio for the samples having different particle sizes are determined. EDX measurements are done at different parts of the samples to ensure the chemical uniformity of the samples. The data undoubtedly disclose almost even chemical homogeneity (Zn/S ratio ~1) of the samples. The EDX data are additionally substantiated employing XPS technique. The Zn/S ratio obtained from XPS data matches well with that of the EDX data.

3.2. ZnS NP Induced Hypoxia and Environmental Acidification

Change in the physicochemical parameters of water due to ZnS NP exposure has been studied at different temperatures when other experimental conditions are kept unaltered. In this study, the dissolved oxygen content in water (DO_2) was measured to be 8.2 mg/L at 15°C before any NP was introduced in it. This value was found to decrease both with increasing NP concentration and with NP exposure time in water at the same temperature. The value of dissolved oxygen content in water reached to a value of as low as 1.2 mg/L for NPs of size 3 nm at a concentration of 1000 µg/L and exposure time of 6 days.

Figure 2 shows the variation of dissolved oxygen content (DO_2) in water at 15°C due to exposure of ZnS NPs of different sizes (d) with increasing NP concentration (σ) for a fixed exposure time (t = 6 days). It is clear from the data that there exists a threshold concentration for σ value in between 150 µg/L and 200 µg/L for each experimental condition. Beyond this value of ZnS NP concentration, a sudden change in DO_2 values can be clearly noticed from the figure. The data in Figure 1 are fitted well with the Boltzmann function depicted by the equation

$$D_{O_2} = a_2 + \frac{(a_1 - a_2)}{1 + e^{(\sigma - \sigma_0)/d\sigma}} \quad (1)$$

Where a_1, a_2 are constants for a particular experimental condition and σ_0 corresponds to the threshold concentration for that specific trial. Examining the fitting parameters it can be inferred definitely that the particles with smaller sizes correspond to the lower value (for d

= 20 nm, σ_0 = 185.06 µg/L; d = 12 nm, σ_0 = 177.29 µg/L; d = 7 nm, σ_0 = 171.13 µg/L; and d = 3 nm, σ_0 = 162.83 µg/L) of threshold concentration.

Figure 3 shows the variation of dissolved oxygen content (DO_2) in water due to exposure of ZnS NPs of different sizes with increasing exposure time (t) for a fixed NP concentration (σ = 500 µg/L). The data are fitted well with the first-order exponential decay curve expressed by the equation

$$D_{O_2} = D^*_{O_2} e^{-t/\tau} \quad (2)$$

Where, $D^*_{O_2}$ is a constant for a fixed trial and τ determines the slope of the curve. Fitting parameters again revealed greater rate of change in D_{O2} value for smaller ZnS NPs. The reduction in dissolved oxygen level in water due to ZnS NP exposure under sunlight can be attributed to their surface photo-oxidation and photoinduced oxygen adsorption properties, which have been significantly enhanced due to the higher surface to volume ratio in NP form. This has been discussed in detail elsewhere [25] using XPS data.

The loss of S from the ZnS NP surface as a result of photo-oxidation creating S vacancies on the NP surface can be established more definitely by studying the Zn 2p and S 2p core-level XPS spectra of the as-synthesized and water exposed ZnS NP samples. Figure 4 shows the Zn 2p core-level XPS spectra of ZnS NPs with an average particle size of 3 nm after a different period of exposure to water under sunlight. As shown in Figure 4, the binding energies of the Zn $2p_{3/2}$ and Zn $2p_{1/2}$ peaks in the as-prepared fresh ZnS NP sample are occurred at about 1021.9 eV and 1045.9 eV, respectively. These values match very well to the standard value [32] for stoichiometric ZnS. Both the peaks show gradual shift to the lower value of binding energies with increasing water exposure time [Figure 4]. Guang *et al.* [33] have attributed the presence of S vacancies on the ZnS NP surface to the lowering of the binding energies of the Zn $2p_{3/2}$ and Zn $2p_{1/2}$ peaks. Wang *et al.* [34] have reported the shifting of Zn $2p_{3/2}$ and Zn $2p_{1/2}$ peaks to the lower values of binding energy with an increase of the S vacancies in the sample. In the present case, the gradual redshift of the Zn $2p_{3/2}$ and Zn $2p_{1/2}$ peaks, therefore, can be safely attributed to the increasing S vacancies with increasing water exposure time due to photo-oxidation of the ZnS NP surface as discussed by Chatterjee *et al*. [25].

Figure 5 shows the S 2p core-level XPS spectra of ZnS NPs having an average size of 3 nm under different experimental conditions, as mentioned in the figure. The binding energy of the S 2p peak in the as-prepared ZnS NP sample is occurred at about 162 eV. This value tallies well to the standard value [32] for stoichiometric ZnS. With increasing the water exposure time, of the peak shows a significant reduction in the intensity and a gradual blue shift in the peaks are also noticed. The reduction in the peak intensity can be associated directly with the loss of S from the NP surface due to photo-oxidation property of ZnS, as discussed above. The Zn/S ratio in ZnS NPs after different periods of water exposure is calculated and shown in Figure 5(inset a). Increasing Zn/S ratio with increasing exposure time is a clear indication of the loss of S from the NP surface due to photo-oxidation property of ZnS.

Figure 5(inset b) shows the blue shift of the S 2p peak at different exposure time. The observed blue shift can be attributed to the photoinduced adsorption of oxygen on the surface of ZnS NPs. The surface of ZnS NP in colloidal dispersion is found to adsorb oxygen under photoirradiation when oxygen is present in the colloidal solution [35]. Removal of atmospheric oxygen is attributed to the photo

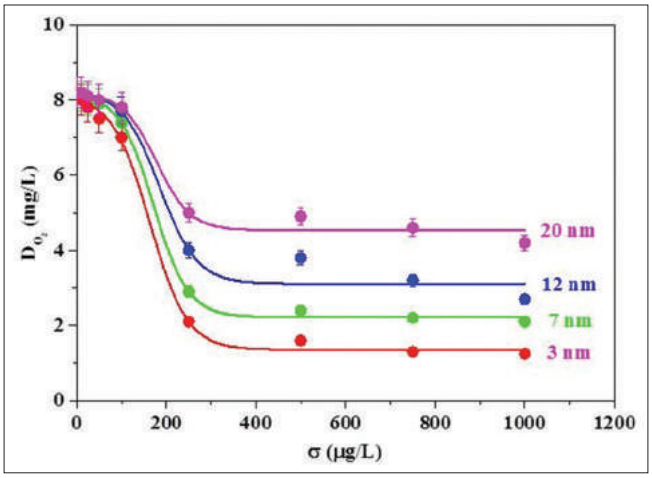

Figure 2: Variation of dissolved oxygen content (DO_2) in water due to exposure of ZnS nanoparticles of different sizes with increasing nanoparticle concentration (σ) for a fixed exposure time (*t* = 6 days).

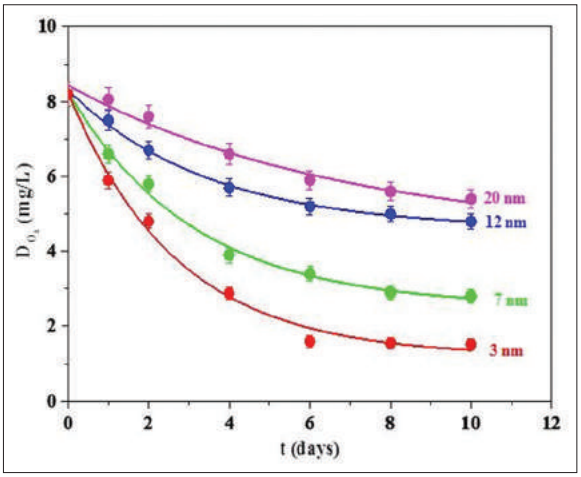

Figure 3: Variation of dissolved oxygen content (DO_2) in water due to exposure of ZnS nanoparticles of different sizes with increasing exposure time (*t*) for a fixed nanoparticle concentration (σ = 500 µg/L).

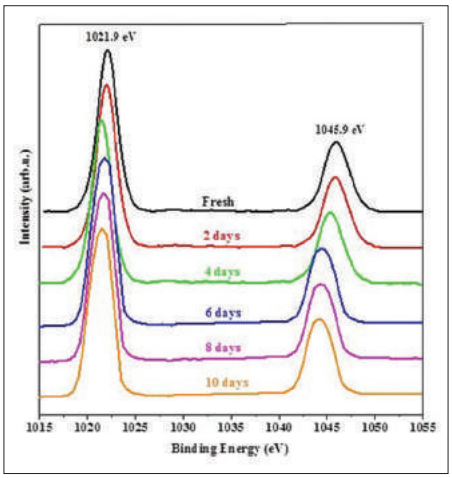

Figure 4: Zn 2p core-level X-ray photoelectron spectroscopic spectra of ZnS nanoparticles with average particle size d=3 nm after a different period of exposure to water under sunlight.

enhanced adsorption of ZnS surface by Kobayashi and Kawaji [36] in case of dry ZnS powders. Both the thermal and radiative processes are identified to lead the chemisorption of oxygen on ZnS surface under apposite experimental conditions [37]. Oxygen adsorption on the ZnS NP surfaces in photo-irradiated ZnS colloidal suspensions possibly befall by the alike photo-enhanced adsorption process [35]. The existence of oxygen or an oxide species on the surface of a colloidal semiconductor ought to have an intense effect on surface recombination of photogenerated electrons and holes. Therefore, the observed blue shift of S 2p XPS peaks with increasing exposure time in the present study can be explained on the basis of the presence of oxygen or an oxygen species on the surface of the ZnS NPs under different experimental conditions.

In this study, the pH value of water was found to decrease when exposed to ZnS NPs in a dose-dependent manner for a fixed exposure time of 6 days. In controlled condition, the pH value of the water used in this experiment was measured to be 7.6. This value was found to decrease both with increasing NP concentration and with NP exposure time in the water for a fixed NP size. The rate of reduction in pH value was found to be higher for the NPs with smaller sizes. In our experiment, the pH value of water dwindled down to 6.2 for NP concentration (σ) of 1000 µg/L with size (d) 3nm and exposure time (t) of 6 days. Reduction of water pH and consequent acidification of the environment finally lead the fishes to metabolic acidosis.

Figure 6 shows the variation of pH value of water (p) due to exposure of ZnS NPs of different sizes with increasing NPs concentration (σ) for a fixed exposure time (t = 6 days). The data shown in this figure are fitted well with the first-order exponential decay curve expressed by the equation

$$p=p_0e^{-\sigma/\tau} \quad (3)$$

Where, p_0 is a constant for a fixed trial and τ determines the slope of the curve. Study on the fitting parameters exposed greater rate of change in pH value due to exposure of smaller ZnS NPs.

Alterations in physicochemical parameters of water were found to be more prominent for ZnS NPs with smaller sizes. This observation could be explained by the fact that smaller particle size culminated higher surface to volume ratio of the NPs present in the water. Therefore, ZnS NPs having smaller sizes offered greater surface area, making the particles more sensitive to surface photo-oxidation process. This leads to a faster deficit in dissolved oxygen content and reduction in pH values when exposed to water compared to the samples having larger particle sizes.

3.3. Impact of ZnS NP Exposure on Liver Function of *L. bata*

The liver is one of the most important organs that participate in the metabolic activity of teleosts. The cell structure of teleost livers is found to respond very sensitively to the environmental changes of their habitat [38]. Consequently, the liver histology of teleosts can be used very effectively to visualize any harmful effect on them due to changes in the atmosphere. Figures 7a-d show the hepatic histology of *L. bata* in a controlled condition and under different experimental conditions. The liver cells are found in normal and healthy states [Figure 7a] for fishes lived under controlled conditions. In this case, large hepatocytes with regular outlines having storage deposits (chiefly composed of glycogen and lipid) are obvious from the micrographs. Centrally located large nuclei indicate the healthy state of the cells. Under this condition, compact tissue layout can be noticed showing almost no empty space in between the cells. Figure 7b-d shows the dose-dependent hazardous effect of ZnS NP on the liver histology of *L. bata*.

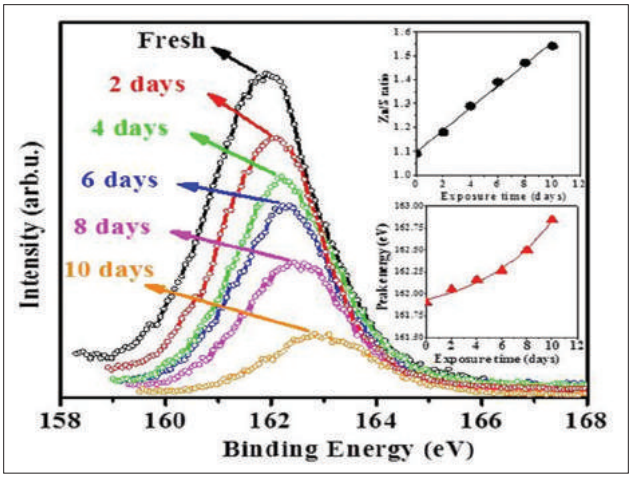

Figure 5: S 2p core-level X-ray photoelectron spectroscopic (XPS) spectra of ZnS nanoparticles with average particle size d = 3 nm after a different period of exposure to water under sunlight. (Inset a) variation of Zn/S ratio calculated for ZnS nanoparticles with water exposure time. (Inset b) variation of peak value of S 2p core-level XPS spectra of ZnS nanoparticles with water exposure time.

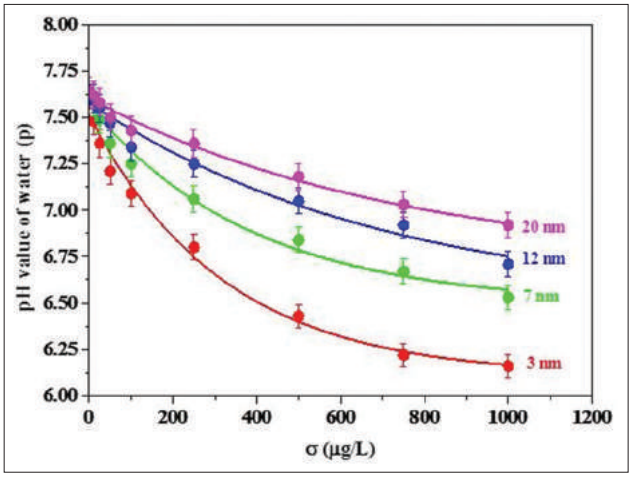

Figure 6: Variation of pH value of water due to exposure of ZnS nanoparticles of different sizes with increasing nanoparticle concentration (σ) for a fixed exposure time (*t* = 6 days).

For exposure to ZnS NP of σ = 100 µg/L [Figure 7b], some cells are noticed to be in the states of degeneration showing no conspicuous nucleus and displaying dispersed cytoplasmic matters. Reduction in hepatocyte sizes due to severe loss of storage deposits can be identified [Figure 7c and d] for exposure to the higher concentration of ZnS NPs. As a result, the nucleus to cell volume ratio is sturdily augmented for the liver cells. Furthermore, hepatocytes are found to be in increasing isolated states having no close contact between them [Figure 7c and d]. Under high concentration exposure of smaller ZnS NPs, some of the livers also show disruption of hepatic cell cords and apoptotic changes such as chromatin condensation and pyknosis as indicated by the green arrows in figures [Figure 7d]. More pronounced histological alterations are found for exposure to NPs of smaller sizes even for same concentration and exposure time.

Figure 8 shows the change in the values hepatic cell diameter (δ) of *L. bata* with increasing NP concentration (σ). δ values are found to

decrease with increase in σ value up to 500 µg/L for every size of the NPs (d) used. Beyond this concentration, this value remains nearly constant. Data are fitted well with first-order exponential decay curves expressed by the equation.

$$\delta = \delta_0 + \alpha e^{\frac{-\sigma}{\tau}} \quad (4)$$

Where δ_0 is the average hepatocyte size without any NP exposure, α is a parameter, and inverse of τ determines the slope of the curve. Therefore, smaller values of τ correspond to the steeper curves. The curve fitting parameters under different experimental conditions are shown in the table [Figure 8, inset]. An investigation on the slopes of the curves establishes undoubtedly that the detrimental effect is stronger for particles with smaller sizes.

3.4. Impact of ZnS NP Exposure on Hematological Parameters of *L. bata*

Figure 9a shows the hematological tissue constitution of *L. bata* under controlled condition. Well-dispersed red blood corpuscles (RBC) are found to be homogeneously distributed throughout. The shapes of the RBC are found to be normal biconvex. Underexposure to ZnS NP concentration of 100 µg/L (d = 3 nm) for 24 days, sticky end and diving RBC are observed in addition to the normal biconvex ones [Figure 9b]. Abnormal polygonal shaped RBC is noticed for exposure of the fish to the ZnS NP concentration of 500 µg/L (d = 3 nm) for 24 days [Figure 9c]. Under the exposure of the highest experimental concentration (σ = 1000 µg/L) of ZnS NP (d = 3 nm) for 24 days, alteration in the arrangement of RBC distribution can be visible [Figure 9d]. Under this condition, RBCs are found to form chain structure in contrast to that monodispersed RBC obtained under controlled condition. Alteration in the layout of the hematological tissue constitution of *L. bata* can be attributed to the acclimatization process of the fish to encounter the ZnS NP induced hypoxia by increasing the oxygen-carrying capacity of blood.

Figure 10a-c shows the variations of hematological parameters recorded in *L. bata* under different experimental conditions. Hb content is found to increase with increasing exposure time (t) [Figure 10a] for t <10 days, when other conditions are kept fixed (d = 3 nm, σ = 1000 µg/L). This parameter is found to rise at a significantly higher level than that of its control value ($P < 0.05$) between t = 6 days and t = 12 days of ZnS NP exposure, having a peak for day t = 10 days. For t > 10 days, this value starts decreasing with increasing t and dwindles down to a lower level compared to the control value for t >16 days. Hemocrit percentage (Hct %) [Figure 10b] and RBC count [Figure 10c] in the fish also show the same type of qualitative variations under increasing ZnS NP exposure time.

This pattern of variation in hematological parameters in *L. bata* can be attributed to its physiological behavior under ZnS NP exposure. Under ZnS induced hypoxia, initially, *L. bata* increases its swimming activity and fast movement to red rid of this hostile condition. This increases the values of these hematological parameters. But for relatively higher time of exposure (t > 12 days), the fish become lethargic and less active. As a result of this, the values of the parameters get reduced. Svobodova *et al.* [39] reported that fish inactive phase display higher values of hematological parameters compared to its less active forms. High RBC values are associated with fast movement, predaceous nature, and high activity with streamlined bodies [40]. This observation is similar to that obtained in the present study.

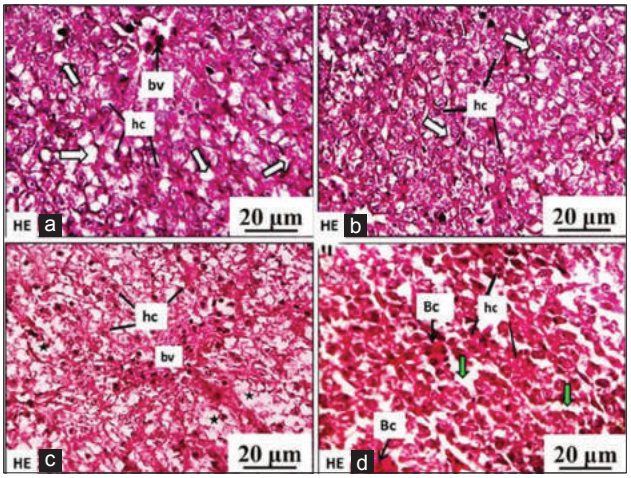

Figure 7: Photomicrographs showing the liver histology of *Labeo bata* under (a) controlled condition, (b) exposure to ZnS NP concentration of σ = 100 µg/L for 6 days, d = 3 nm, (c) exposure to ZnS NP concentration of σ = 500 µg/L for 6 days, d = 3 nm and (d) exposure to ZnS NP concentration of σ = 1000 µg/L for 6 days, d = 3 nm. In this case, livers tissues showed disruption of hepatic cell cords and apoptotic changes such as chromatin condensation and pyknosis as indicated by green block arrows in figure (hepatocytes [hc], fat vacuoles [fv-white block arrows], blood vessels [Bv], empty space generated due to apoptosis [★], and blood cells [Bc]).

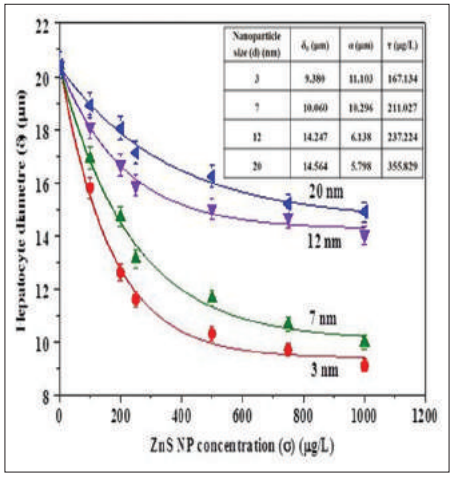

Figure 8: Change in the values hepatic cell diameter (δ) of *Labeo bata* with increasing nanoparticle concentration (σ) along with theoretical fitted curves and fitting parameters in inset table.

3.5. Impact of ZnS NP exposure on metabolic parameters of *L. bata*

Table 1 summarizes the variations of metabolic parameters recorded in *L. bata* under different experimental conditions. Blood glucose levels of the fish are found to increase initially for smaller exposure time (6, 12 days) over the control value ($P < 0.05$) and then ($t > 12$ days) found to reduce significantly ($P < 0.05$) than that of the control value with increasing time of ZnS NP exposure. This variation pattern of glucose level in *L. bata* can be associated with its physiological behavior under ZnS NP exposure. In this study, initial rise and then subsequent fall of blood glucose level in *L. bata* with increasing ZnS NP exposure time suggests that the prolong hypoxia perhaps affects the glucose sensing system of the fish.

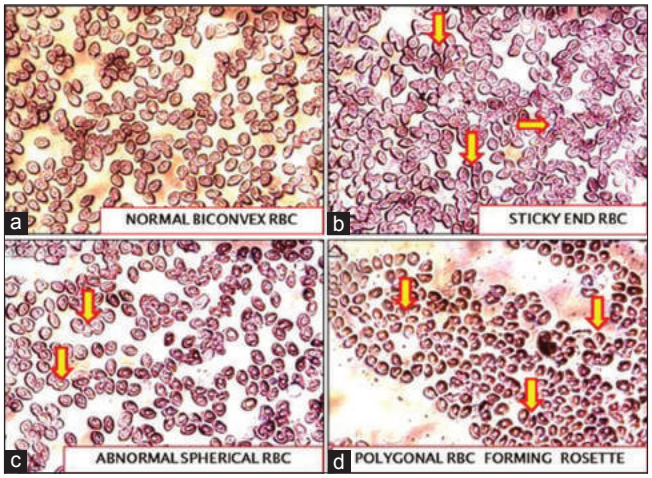

Figure 9: Photomicrographs showing the hematological tissue constitution of female *L. bata* under (a) controlled condition, (b) exposure to ZnS NP concentration of σ = 100 µg/L for 24 days, d = 3 nm, (c) exposure to ZnS NP concentration of σ = 500 µg/L for 24 days, d = 3 nm, and (d) exposure to ZnS NP concentration of σ = 1000 µg/L for 24 days, d = 3 nm. (magnification ×600) (Leishman stain).

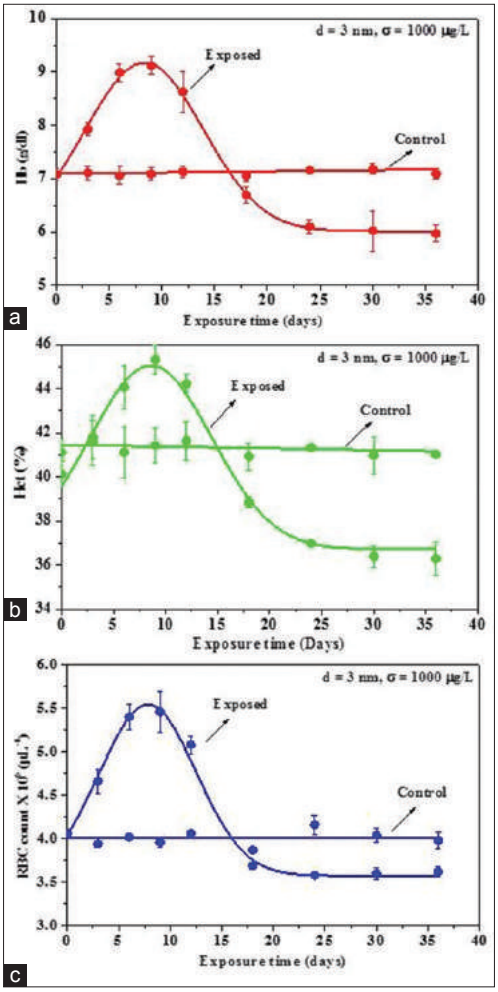

Figure 10: Variation of (a) hemoglobin (Hb) content, (b) hemocrit percentage (Hct %), and (c) red blood corpuscle count, recorded in *Labeo bata* under different experimental conditions.

Table 1: The metabolic parameters recorded in *L. bata* under ZnS nanoparticle exposure (d=3 nm, σ = 1000 µg/L) for different exposure times (*t*=6, 12, 18, and 24 days) (Data shown are mean values±SE, * denotes the data are significantly different from control [when $P<0.05$])

Metabolic parameters	Exposure time (in days)	Control	Experiment
Blood glucose level (mg/dL)	6	140.50±0.03	148.0±0.08*
	12	139.89±0.10	156.0±0.12*
	18	140.78±0.93	138.0±0.58
	24	140.34±0.93	132.0±0.24*
Blood lactate level (mmol/L)	6	6.12±0.06	8.00±0.04*
	12	6.08±0.11	9.02±0.11*
	18	6.54±0.02	4.76±0.43*
	24	6.38±0.13	3.43±0.89*

Blood lactate level of the fish is found to increase initially for smaller exposure time (6, 12 days) over the control value ($P < 0.05$) and then ($t > 12$ days) found to reduce significantly ($P < 0.05$) than that of the control value with increasing time of ZnS NP exposure. This variation pattern of variation of blood lactate level in *L. bata* can also be associated with its physiological behavior under ZnS NP exposure. Blood lactate concentrations are found to be higher in more active phase of fish, compared to the phase when it is less active [41]. High-speed movements require an enhancement in the muscular activity. When this surpasses the capability of the circulatory system to carry oxygen to the respective tissues, the anaerobic metabolism complements the aerobic metabolism [41,42]. The ability of anaerobic energy formation can be appraised from diminutions in substrate reserves and product accretion with the transformation of glucose to lactate. It is soon followed by the increase in pyruvate metabolism and debt of oxygen [43-46]. These observations are in agreement with the present study.

4. CONCLUSION

The dissolved oxygen content in water is found to reduce in a dose-dependent manner when ZnS NPs are exposed to the water under sunlight due to enhanced photo-oxidation property of ZnS in its NP form. Being forced to live in an oxygen depleted atmosphere, the physiological behaviors of *L. bata* is significantly changed. Due to the minimization of food intake, the hepatic cells of the fish are found to reduce in sizes as they use the storage deposits to maintain the most essential physiological and metabolic activities required for survival. For relatively smaller exposure time a significant increase in the number density of red blood corpuscles (RBC) is documented. Under hypoxia condition, Hb and hematocrit concentrations are found to increase initially, showing a physiological adaptation to enhance oxygen transport capacity. Blood glucose and blood lactate levels of *L. bata* vary accordingly to the varied physiological behavior of the fish under ZnS NP exposure. These observations suggest that *L. bata* is able to respond against ZnS NP induced hypoxia through increasing its internal oxygen carrying capacity and leading itself to a comparatively sedentary lifestyle as survival strategies.

5. ACKNOWLEDGMENT

The authors sincerely acknowledge Professor Chung –Hsin Lu, Department of Chemical Engineering, National Taiwan University,

Taipei, Taiwan, for helping them to characterize ZnS NP through different characterization techniques.

REFERENCES

1. Aitken RJ, Chaudhry MQ, Boxall AB, Hull M. Manufacture and use of nanomaterials: Current status in the UK and global trends. Occup Med (Lond) 2006;56:300-6.
2. Brody AL. Nano and food packaging technologies converge. Food Technol 2006;60:92-4.
3. Karnik BS, Davies SH, Baumann MJ, Masten SJ. Fabrication of catalytic membranes for the treatment of drinking water using combined ozonation and ultrafiltration. Environ Sci Technol 2005;39:7656-61.
4. Carlson C, Hussain SM, Schrand AM, Braydich-Stolle LK, Hess KL, Jones RL, *et al.* Unique cellular interaction of silver nanoparticles: Size-dependent generation of reactive oxygen species. J Phys Chem B 2008;112:13608-19.
5. Ispas C, Andreescu D, Patel A, Goia DV, Andreescu S, Wallace KN. Toxicity and developmental defects of different sizes and shape nickel nanoparticles in zebrafish. Environ Sci Technol 2009;43:6349-56.
6. Mironava T, Hadjiargyrou M, Simon M, Jurukovski V, Rafailovich MH. Gold nanoparticles cellular toxicity and recovery: Effect of size, concentration and exposure time. Nanotoxicology 2010;4:120-37.
7. Pelkmans L, Helenius A. Endocytosis *via* caveolae. Traffic 2002;3:311-20.
8. Rejman J, Oberle V, Zuhorn IS, Hoekstra D. Size-dependent internalization of particles *via* the pathways of clathrin- and caveolae-mediated endocytosis. Biochem J 2004;377:159-69.
9. Moore MN. Lysosomal cytochemistry in marine environmental monitoring. Histochem J 1990;22:187-91.
10. Adams LK, Lyon DY, Alvarez PJ. Comparative ecotoxicity of nanoscale TiO_2, SiO_2, and ZnO water suspensions. Water Res 2006;40:3527-32.
11. Warheit D, Everitt J. Assessing the biological and environmental risks of nanoparticles. Proceedings of the 43rd Society of Toxicology Annual Meeting, Baltimore, MD, USA; 2004. p. 1850.
12. Warheit DB, Laurence BR, Reed KL, Roach DH, Reynolds GA, Webb TR. Comparative pulmonary toxicity assessment of single-wall carbon nanotubes in rats. Toxicol Sci 2004;77:117-25.
13. Tong Z, Bischoff M, Nies L, Applegate B, Turco RF. Impact of fullerene (C_{60}) on a soil microbial community. Environ Sci Technol 2007;41:2985-91.
14. Fang JD, Lyon Y, Wiesner MR, Dong J, Alvarez PJ. Effect of a fullerene water suspension on bacterial phospholipids and membrane phase behaviour. Environ Sci Technol 2007;41:2636-42.
15. Smith CJ, Shaw BJ, Handy RD. Toxicity of single walled carbon nanotubes to rainbow trout, (*Oncorhynchus mykiss*): Respiratory toxicity, organ pathologies, and other physiological effects. Aquatic Toxicol 2007;82:94-109.
16. Oberdörster E. Manufactured nanomaterials (fullerenes, C_{60}) induce oxidative stress in the brain of juvenile largemouth bass. Environ Health Perspect 2004;112:1058-62.
17. Koziara JM, Lockman PR, Allen DD, Mumper RJ. *In situ* blood-brain barrier transport of nanoparticles. Pharm Res 2003;20:1772-8.
18. Lyon DY, Adams LK, Falkner JC, Alvarezt PJ. Antibacterial activity of fullerene water suspensions: Effects of preparation method and particle size. Environ Sci Technol 2006;40:4360-6.
19. Lyon DY, Fortner JD, Sayes CM, Colvin VL, Hughes JB. Bacterial cell association and antimicrobial activity of a C_{60} water suspension. Environ Toxicol Chem 2005;24:2757-62.
20. Oberdörster E, Zhu S, Blickley TM, McClellan-Green P, Haasch ML. Ecotoxicology of carbon-based engineered nanoparticles: Effects of fullerene (C_{60}) on aquatic organisms. Carbon 2006;44:1112-20.
21. Zhu SQ, Oberdörster E, Haasch ML. Toxicity of an engineered nanoparticle (fullerene, C_{60}) in two aquatic species, *Daphnia* and fathead minnow. Mar Environ Res 2006;62:S5-9.
22. Griffitt RJ, Weil R, Hyndman KA, Denslow ND, Powers K, Taylor D, *et al.* Exposure to copper nanoparticles causes gill injury and acute lethality in zebrafish (*Danio rerio*). Environ Sci Technol 2007;41:8178-86.
23. Federici G, Shaw BJ, Handy RD. Toxicity of titanium dioxide nanoparticles to rainbow trout (*Oncorhynchus mykiss*): Gill injury, oxidative stress, and other physiological effects. Aquat Toxicol 2007;84:415-30.
24. Bhattacharjee B, Chatterjee N, Lu CH. Harmful impact of ZnS nanoparticles on *Daphnia sp.* in the western part (districts of Bankura and Purulia) of West Bengal, India. ISRN Nanomater 2013;2013:207239.
25. Chatterjee N, Bhattacharjee B, Lu CH. Hazardous effect of ZnS nanoparticles on the feeding behaviour, growth and maturation process of the Asian striped catfish, *Mystus vittatus* (Bloch, 1794). Int Aquatic Res 2014;6:71-82.
26. Chatterjee N, Bhattacharjee B. Changing physicochemical properties of water due to exposure of ZnS nanoparticles and its detrimental effect on feeding behaviour and liver of a non-air breathing catfish *Mystus vittatus*. Int J Latest Res Sci Technol 2014;3:199-204.
27. Chatterjee N, Bhattacharjee B. Salient alterations in hepatic and renal histomorphology of an Indian minor carp, *Labeo bata* (Hamilton, 1822) owing to ZnS nanoparticle induced hypoxia and environmental acidification. Int J Earth Environ Sci 2015;1:1-9.
28. Chatterjee N, Bhattacharjee B. An analytic contemplation on the conspicuous vicissitudes in the histomorphology of corpuscles of stannius of a fresh water catfish *Mystus tengara* (Hamilton, 1822) due to the exposure of ZnS nanoparticles. Scientifica 2015;2015:697053.
29. Chatterjee N, Bhattacharjee B. ZnS nanoparticles affect hazardously the process of oogenesis in the dwarf Asian striped catfish *Mystus vittatus* (Bloch, 1794). Adv Sci Lett 2016;22:126-31.
30. Chatterjee N, Bhattacharjee B. Revelation of ZnS nanoparticles induce follicular atresia and apoptosis in the ovarian preovulatory follicles in the catfish *Mystus tengara* (Hamilton, 1822). Scientifica 2016;2016:3927340.
31. Bhattacharjee B, Chatterjee N. Perilous effect of ZnS nanoparticles on testicular cell development and sperm morphology in the Asian striped catfish *Mystus vittatus* (Bloch, 1794). Adv Sci Lett 2016;22:64-70.
32. Moulder JF, Stickle WF, Sobol PE, Bomren KD. Handbook of X-Ray Photoelectron Spectroscopy. Minnesota, USA: Physical Electronics, Inc.; 1995.
33. Guan M, Xiao C, Zhang J, Fan S, An R, Cheng Q, *et al.* Vacancy associates promoting solar-driven photocatalytic activity of ultrathin bismuth oxychloride nanosheets. J Am Chem Soc 2013;135:10411-7.
34. Wang G, Huang B, Li Z, Lou Z, Wang Z, Dai Y, *et al.* Synthesis and characterization of ZnS with controlled amount of S vacancies for photocatalytic H2 production under visible light. Sci Rep 2015;5:8544.
35. Becker WG, Bard AJ. Photoluminescence and photoinduced oxygen adsorption of colloidal zinc sulphide dispersions. J Phys Chem 1983;87:4888-93.
36. Kobayashi A, Kawaji S. Adsorption and surface potential of semi-conductors. Part 1. Photo-enhanced adsorption of oxygen and change of contact potential of ZnS phosphors with illumination. J Phys Soc Jpn 1955;10:270-3.
37. Muminov MI, Kim GC, Zaitov FA, Kalamozov RU. Some features of the chemisorption of oxygen on semiconductors with different widths of the forbidden band. Dokl Akad Nauk Uzb SSR 1975;12:20-1.
38. Segner H, Möller H. Electron microscopical investigations on

starvation induced liver pathology in flounders *Platichthys flesus*. Mar Ecol Prog Ser 1984;19:193-6.
39. Svobodova Z, Kroupova H, Modra H, Flajshans M, Randak T, Savina LV, *et al*. Haematological profile of common carp spawners of various breeds. J Appl Ichthyol 2008;24:55-9.
40. Rambhaskar B, Rao KS. Comparative haematology of ten species of marine fish from Visakhapatnam coast. J Fish Biol 1987;30:59-66.
41. Heath AG, Pritchard AW. Changes in the metabolic rate and blood lactic acid of blue gill sun fish, *Lepomis macrochirus* following severe muscular activity. Physiol Zool 1962;38:767-76.
42. Brett JR. The metabolic demand for oxygen in fish, particularly salmonids, and a comparison with other vertebrates. Respir Physiol 1972;14:151-70.
43. Puckett KJ, Dill LM. Cost of sustained and burst swimming to juvenile Coho salmon (*Oncorhynchus kisutch*). Can J Fisheries Aquatic Sci 1984;41:1546-51.
44. Puckett KJ, Dill LM. The energetics of feeding territorially in Juvenile Coho salmon (*Oncorhynchus kisutch*). Behaviour 1985;92:97-111.
45. Kauffman R. Respiratory cost of swimming in larval and juvenile cyprinids. J Exp Biol 1990;150:343-66.
46. Goolish EM. Aerobic and anaerobic scaling in fish. Biol Rev Camb Philos Soc 1991;66:33-56.

How to cite this article:
Chatterjee N, Bhattacharjee B. ZnS nanoparticles persuade alterations in metabolic and hematological aspects in the cyprinid *Labeo bata* (Hamilton, 1822). J App Biol Biotech. 2018;6(2):6-14.
DOI: 10.7324/JABB.2018.60202